THE JOURNAL OF BIOLOGICAL CHEMISTRY VOL. 287, NO. 50, pp. 41706–41719, December 7, 2012

Regulator of G-protein Signaling-21 (RGS21) Is an Inhibitor of Bitter Gustatory Signaling Found in Lingual and Airway Epithelia*

Received for publication, September 28, 2012, and in revised form, October 22, 2012 Published, JBC Papers in Press, October 24, 2012, DOI 10.1074/jbc.M112.423806

Staci P. Cohen[‡], Brian K. Buckley[‡], Mickey Kosloff[§¶], Alaina L. Garland[‖], Dustin E. Bosch[‡], JrGang Cheng[**], Harish Radhakrishna[‡‡1], Michael D. Brown[‡‡], Francis S. Willard[‡2], Vadim Y. Arshavsky[§], Robert Tarran[‖], David P. Siderovski[‡3], and Adam J. Kimple[‡]

From the Departments of [‡]Pharmacology and [‖]Cell and Molecular Physiology, [‖]CF/Pulmonary Research and Treatment Center, and [**]University of North Carolina Neuroscience Center, University of North Carolina, Chapel Hill, North Carolina 27599-7365, the [§]Duke Eye Center, Duke University Medical Center, Durham, North Carolina 27710, the [¶]Department of Biology, Faculty of Natural Sciences, University of Haifa, Haifa 31905, Israel, and the [‡‡]Department of Biosciences, The Coca-Cola Company, Atlanta, Georgia 30313

Background: RGS21 is expressed in tastant-responsive lingual epithelium, but with unknown function.
Results: RGS21 accelerated intrinsic GTPase activity of multiple Gα subunits; RGS21 over- and underexpression in epithelial cells modulated bitterant responsiveness.
Conclusion: RGS21 is a negative regulator of bitterant signal transduction.
Significance: RGS21 represents a nonreceptor regulatory component of gustatory signaling that alters sensitivity of bitterant responsiveness in an endogenous, cellular context.

The gustatory system detects tastants and transmits signals to the brain regarding ingested substances and nutrients. Although tastant receptors and taste signaling pathways have been identified, little is known about their regulation. Because bitter, sweet, and umami taste receptors are G protein-coupled receptors (GPCRs), we hypothesized that regulators of G protein signaling (RGS) proteins may be involved. The recent cloning of RGS21 from taste bud cells has implicated this protein in the regulation of taste signaling; however, the exact role of RGS21 has not been precisely defined. Here, we sought to determine the role of RGS21 in tastant responsiveness. Biochemical analyses confirmed *in silico* predictions that RGS21 acts as a GTPase-accelerating protein (GAP) for multiple G protein α subunits, including adenylyl cyclase-inhibitory ($G\alpha_i$) subunits and those thought to be involved in tastant signal transduction. Using a combination of *in situ* hybridization, RT-PCR, immunohistochemistry, and immunofluorescence, we demonstrate that RGS21 is not only endogenously expressed in mouse taste buds but also in lung airway epithelial cells, which have previously been shown to express components of the taste signaling cascade. Furthermore, as shown by reverse transcription-PCR, the immortalized human airway cell line 16HBE was found to express transcripts for tastant receptors, RGS21, and downstream taste signaling components. Over- and underexpression of RGS21 in 16HBE cells confirmed that RGS21 acts to oppose bitter tastant signaling to cAMP and calcium second messenger changes. Our data collectively suggests that RGS21 modulates bitter taste signal transduction.

G protein-coupled receptors (GPCRs)[4] are a family of seven transmembrane domain, cell-surface proteins that mediate diverse cellular functions, from the perception of light and odor to the physiologic effects of hormones and neurotransmitters (1–3). These receptors are coupled to secondary messenger systems by heterotrimeric G proteins, consisting of α, β, and γ subunits. Gβ and Gγ form an obligate heterodimer that binds to GDP-bound Gα. Upon binding extracellular ligand, such as a tastant, the GPCR acts as a guanine nucleotide exchange factor, promoting release of GDP from Gα (4). Nucleotide-free Gα then binds GTP and releases Gβγ (5). Both Gα·GTP and freed Gβγ are then capable of modulating downstream effectors (ion channels, enzymes) specific to each heterotrimer subtype and cellular context (6–8). Intrinsic GTPase activity of Gα returns it to the GDP-bound state, allowing re-formation of the Gα·GDP/Gβγ heterotrimer. This reassociation terminates effector interactions (9). Thus, the duration of GPCR signaling is determined by the lifetime of Gα in the GTP-bound state. However, the rate of intrinsic GTP hydrolysis by Gα observed *in vitro* rarely accounts for the speed of GPCR signaling decay *in vivo* (9, 10). Several groups (11–14) simultaneously discovered the "regulators of G protein signaling" (RGS proteins), a superfamily of proteins that dramatically increase the rate of GTP

* This work was supported, in whole or in part, by National Institutes of Health Grants R01 GM082892 (to D. P. S.), R01 HL108927 (to R. T.), R01 EY012859 (to V. Y. A.), and National Institutes of Health/NIDCD Ruth L. Kirschstein NRSA Fellowship F32 DC011670 (to S. P. C.).
[1] Present address: Chromocell Corp., North Brunswick, NJ.
[2] Present address: Lilly Research Laboratories, Eli Lilly and Co., Indianapolis, IN.
[3] To whom correspondence should be addressed: 3051A Health Sciences North, One Medical Center Dr., Robert C. Byrd Health Sciences Center, Morgantown, WV 26506-9229. Tel.: 304-293-4991; E-mail: dpsiderovski@hsc.wvu.edu.

[4] The abbreviations used are: GPCR, G protein-coupled receptor; RGS, regulator of G protein signaling; PLC, phospholipase C; MTE, mouse tracheal epithelia; FLIPR, fluorescence imaging plate reader; BAC, bacterial artificial chromosome; SPR, surface plasmon resonance; CI, confidence interval; qRT, quantitative reverse transcription.

hydrolysis by Gα subunits and thereby determine the duration of GPCR signaling (15). For example, in the mammalian visual system controlled by the GPCR rhodopsin, the time constant at which rod photoreceptor cells recover from flash response increases from 0.2 s (wild-type) to 9 s in RGS9-deficient mice (16), clearly highlighting the importance of RGS proteins to proper signal transduction timing (17).

The T1R and T2R families of GPCRs compose the mammalian taste receptors that detect the taste modalities of umami, sweet, and bitter (18). The T2R family is responsible for transduction of bitter taste (19, 20). In contrast to the T2R receptors, which are functional when expressed individually, T1Rs only function when expressed as heterodimers (21, 22). L-Amino acids (umami compounds) signal through the T1R1-T1R3 heterodimer (22). Similarly, sweet compounds bind to the T1R2-T1R3 heterodimer to initiate taste signaling (21).

Perception of bitterness by the gustatory system helps to identify toxic or spoiled foods that should not be ingested; however, many nonharmful compounds also are perceived as bitter, including some artificial sweeteners and many medicines (23–30). Tastant receptors have also been identified outside the gustatory system, including bitter receptors in ciliated epithelial airway and enteroendocrine cells (31–34), but their function in these tissues is still being determined. Understanding the physiological regulation of these signaling pathways should lead to the development of more palatable therapeutics and artificial sweeteners, as well as better glucose modulators.

The critical components of taste transduction downstream of the T1R and T2R receptors are slowly being elucidated. Similar to the visual system, which has two unique Gα subunits specific for rods and cones, lingual taste cells also have a unique Gα called gustducin-α (encoded by *GNAT3*), which is highly related by sequence to rod transducin ($G\alpha_{t\text{-}rod}$, encoded by *GNAT1*) (35). Gustducin has a critical role in the transduction of bitter and sweet taste (36); however, the appetitive effects of umami compounds are only lost when animals are deficient in both gustducin-α and $G\alpha_{t\text{-}rod}$ (37), suggesting some degree of functional redundancy. Although gustducin and transducin are widely accepted to be the critical Gα subunits in mediating taste in lingual tissue (36, 37), the role of other Gα subunits remains unknown. The ability of gustducin-α/transducin double knockout mice to still produce recordable action potentials on chorda tympani recordings upon exposure to bitter tastants (37), and the high levels of $G\alpha_{i2}$ expressed in lingual taste cells (38), suggests that $G\alpha_{i2}$ may also have a role in taste transduction (37, 39).

Although knock-out mice have shown the importance of gustducin and transducin to gustation signal transduction, downstream second messenger systems have also been implicated. Tastant-dependent heterotrimer activation is seen to rapidly change cyclic nucleotide levels (including cAMP) in a phosphodiesterase-dependent manner, but a physiological role of these changes remains unsupported by direct evidence (40). Tastant receptor activation also results in a PLC-β2-mediated increase in intracellular calcium and subsequent gating of the taste-transduction channel TRPM5. Both PLC-β2-null and TRPM5-null mouse strains have reduced or a complete loss of bitter, sweet, and umami signaling (41, 42).

Although multiple intracellular modulators are known to regulate G protein activity and GPCR-initiated signaling (43, 44), modulators specific to tastant signal transduction are only now being identified (*e.g.* Refs. 45 and 46). Two independent groups identified a novel member of the RGS protein family, RGS21, that may be involved in tastant signal transduction based on its expression in lingual taste-responsive epithelium (47, 48). Using *in situ* hybridization and RT-PCR, RGS21 expression was identified only in a subset of taste bud cells in one study (47), yet found in every tissue screened in the other (48). Neither report established the specific function of RGS21 in tastant signal transduction (47, 48). Thus, our present study aimed to clarify the discordant reports of RGS21 expression and define its role in tastant signaling, thereby furthering our collective understanding of the physiological modulation of taste perception.

EXPERIMENTAL PROCEDURES

Chemicals and Assay Materials

Unless otherwise noted, all chemicals were the highest grade available from Sigma or Fisher Scientific (Pittsburgh, PA).

Reverse Transcription-Polymerase Chain Reaction (RT-PCR)

RNA Isolation—Cells from lung epithelial cell lines were stored in RNase-free PBS at −20 °C for up to 16 h before use. RNA isolations were performed in an RNA purification tray, using the ABI Prism 6700 automated nucleic acid work station (PE Biosystems) and following the manufacturer's protocol. Total RNA samples were stored at −20 °C.

Primers and Probes—The nucleotide sequences of the PCR primers and their fluorogenic probes for the target genes were designed by using the computer program Primer Express (PE Biosystems). Each fluorescent probe had a reporter dye (FAM for the target RNA and TET for the 18 S RNA control) covalently attached at its 5′ end and a quencher dye (TAMRA) attached at its 3′ end. Before use, the probes were purified by a PolyPak II cartridge (Glen Research, Sterling, VA) following the manufacturer's instructions.

RT-PCR Amplifications—Real-time RT-PCR amplifications were performed in a 96-well plate in an ABI Prism 7700 sequence detector (PE Biosystems) in a total volume of 30 μl, which included 10 μl of RNA sample from the ABI Prism 6700 plus 20 μl of a reaction mixture made with minor modifications of the manufacturer's instructions. Each RT-PCR amplification was performed in triplicate: 30 min at 48 °C for the RT reaction, then 10 min at 94 °C, followed by a total of 40 temperature cycles (15 s at 94 °C and 1 min at 60 °C). During the amplification, the fluorescence of FAM (or TET), TAMRA, and ROX (a passive reference dye) was measured by the 7700 Sequence Detector in each well of the 96-well plate. The cycle numbers at which the fluorescence of the PCR starting samples crossed a set threshold (C_t) were calculated by using the sequence detector software incorporated in the ABI Prism 7700 Sequence Detector System.

Relative Quantification of Gene Expression—Amplification of the 18S RNA gene was used as an endogenous control. For each experimental sample, the relative amounts of the target and endogenous control were determined from the C_t. We

assume that 18S RNA is present in all tested samples of cell RNA at a constant proportion and therefore normalized the amount of total RNA in our test samples by comparing the C_t of their 18S RNA with that of our test genes. For each gene, the data were then expressed as a percentage of the cell line with the highest normalized C_t (49).

In Situ Hybridization

cDNA spans from the mouse *Rgs21* open reading frame (full-length), *PLCβ2* (nucleotides 227–740), and *gustducin-α* (nucleotides 83–610) were separately cloned into pBluescript II SK (Stratagene) using the KpnI and NotI digestion sites. Digoxigenin-labeled riboprobes were generated using T7 RNA polymerase and a digoxigenin-RNA labeling mix (Roche Applied Science). Hybridization was performed by the University of North Carolina (UNC) Neuroscience Center *In Situ* Hybridization Core according to standard protocols (UNC-Chapel Hill).

Generation of Rgs21::RFP BAC Transgenic Mice

A 232-kilobase bacterial artificial chromosome (BAC) from mouse chromosome 1 (RP23–126D12: nucleotides 146,254,848 to 146,486,740) that encodes TagRFP (50) driven by the *Rgs21* promoter was engineered by BAC recombineering and purified by pulsed field electrophoresis by the UNC Neuroscience Center BAC Engineering Core Facility. Pronuclear injections were performed by the UNC Animal Models Core on C57Bl/6XDBA2 hybrid embryos, which were subsequently implanted into pseudo-pregnant recipient females. Resultant pups were genotyped via tail biopsies at 21 days to confirm gene expression, and *Rgs21*::RFP BAC-transgenic founder mice were established. *Rgs21*::RFP BAC transgenic mice were bred with wild-type C57Bl/6J mice and the resulting F1 pups were utilized in this study. All animal protocols received prior approval by the Institutional Animal Care and Use Committee (IACUC) of UNC-Chapel Hill and all animals were cared for in an AAALAC-accredited vivarium according to NIH standards.

Immunofluorescence

Mouse tongues were removed post-humane euthanasia and fixed in 4% paraformaldehyde at 4 °C overnight, followed by an overnight incubation in 30% sucrose at 4 °C. Circumvallate papillae were then dissected from these fixed tongues, embedded, and frozen in Tissue-Tek OCT compound (Fisher Scientific), and coronally sectioned (12 μm thick) at −22 °C. Circumvallate papillae sections were mounted on FisherBrand SuperfrostPlus slides and permeabilized with 0.5% Triton X-100 in phosphate-buffered saline (PBS) for 1 h at room temperature. These slides were incubated in blocking buffer (0.5% Triton X-100 and 1% bovine serum albumin in PBS) for an additional hour at room temperature and then probed overnight at 4 °C with rabbit anti-gustducin-α polyclonal primary antibody (sc-395; Santa Cruz) diluted in blocking buffer. After 4 washes in PBS, slides were incubated again for 30 min in blocking buffer and then probed for 1 h at room temperature with Alexa Fluor-488 goat anti-rabbit IgG (heavy and light chains) secondary antibody (Invitrogen) diluted in blocking buffer. Slides were then washed 4 times in PBS. Vectashield mounting medium with DAPI (Vector Labs) was applied to mount glass coverslips onto the slides. Immunofluorescence was detected with an IX70 epifluorescence microscope (Olympus) and mounted digital camera (Hamamatsu). Images were digitally processed and pseudocolored using Adobe Illustrator CS4 software.

Cloning

The RGS21 open reading frame (ORF) was cloned by PCR from cDNA isolated from rat taste bud cell (a gift from Dr. Lars von Buchholtz, NIH/NIDCR) using the sense primer, 5′-CCAGTGAAATGCTGTTTCTAC-3′ and antisense primer, 5′-CAGGAAAGGCAGCCATC-3′ with an annealing temperature of 52 °C and an extension time of 22 s using Phusion thermostable DNA polymerase (New England Biolabs, Ipswich, MA). Following amplification, a 453-bp band was resolved using agarose electrophoresis and isolated by Qiagen Gel Extraction (Qiagen). A second round of PCR, using primers to extend the RGS21 ORF sequence, was used to subclone the isolated fragment into a pET-based (Novagen) ligation-independent cloning vector to make a tobacco etch virus protease-cleavable His_6 fusion protein for expression in *Escherichia coli*, as well as into a pcDNA3.1-based (Invitrogen) ligation-independent cloning vector to make a hemagglutinin (HA)-epitope fusion protein for expression in mammalian cells, both as previously described (51, 52). QuikChange site-directed mutagenesis (Stratagene) was used to mutate Arg-126 of the RGS21 ORF to a glutamic acid codon (R126E) with sense primer, 5′-gtctcatggccaaggattccttccctgagtttctaaagtcagaaatttataagaaa-3′ and antisense primer, 5′-tttcttataaatttctgactttagaaactcagggaaggaatccttggccatgagac-3′.

Protein Expression and Purification

The pET-based vector encoding the His_6-rRGS21(wild type) or -RGS21(R126E) ORF was transformed into *E. coli* BL21(DE3) cells (Novagen) and grown at 37 °C in Luria broth until a culture density of A_{600} = 0.75 was reached. Protein expression was then induced by addition of 0.75 mM isopropyl β-D-thiogalactopyranoside. After culture for 14–16 h at 20 °C, cells were pelleted by centrifugation and frozen at −80 °C. Prior to purification, bacterial cell pellets were resuspended in N1 buffer (50 mM Tris, pH 7.5, 300 mM NaCl, 30 mM imidazole, 5% (w/v) glycerol) for lysis using high-pressure homogenization with an Emulsiflex (Avestin, Ottawa, Canada). Cellular lysates were clarified by centrifugation for 45 min at 100,000 × *g* at 4 °C before the supernatant was applied to a nickel-nitrilotriacetic acid resin FPLC column (FF HisTrap; GE Healthcare). The column was washed with 7 column volumes of N1 lacking imidazole, then 3 column volumes of N1 containing 30 mM imidazole, 5 column volumes of N1 containing 300 mM imidazole, and 5 column volumes of N1 containing 700 mM imidazole. Soluble RGS21 protein was found in the 300 mM imidazole-containing fractions. The column flow-through was pooled and resolved using a calibrated 150-ml size exclusion column (Sephacryl S200, GE Healthcare) with S200 buffer (50 mM Tris, pH 7.5, 150 mM NaCl, 5% (w/v) glycerol). Protein was concentrated to ~1 mM as determined by $A_{280\ nm}$ measurements upon denaturation in guanidine hydrochloride. Circular dichroism spectra were separately collected using 0.1 mg/ml of RGS21 and

RGS21(R126E) proteins, each diluted in 10 mM potassium phosphate salt, pH 7.5, at 25 °C using a PiStar-180 spectrophotometer (Applied Photophysics, UK) within the University of North Carolina Macromolecular Interactions Facility (Dr. Ash Tripathy, director). Spectra were collected from 185 to 260 nm in 0.5-nm steps with a bandwidth of 2 nm.

His_6-$G\alpha_{oA}$ was purified using a similar chromatographic methods as previously described (53). His_6-$G\alpha_{i1,i2,i3}$ and His_6-$G\alpha_{i1}$(G183S) subunits were purified exactly as previously described for the production of $G\alpha_{i1}$ (54). The His_6-$G\alpha_{t/i1}$ chimeric Gα subunit ("Chi6") was purified as previously described (55) and Gα-transducin was purified from bovine rod outer segments as previously described (56).

Cell Culture and Co-immunoprecipitation

COS-7 cells and the human bronchial airway epithelial cell line 16HBE were separately cultured in Dulbecco's modified Eagle's medium (Invitrogen) supplemented with 10% fetal bovine serum (Denville Scientific, Metuchen, NJ) and penicillin-streptomycin (Mediatech, Inc., Manassas, VA) and maintained at 37 °C in a humidified atmosphere containing 5% CO_2. COS7 cells were plated in 6-well dishes and transfected with 1.5 μg of DNA (when at 70% confluence) with Lipofectamine™ 2000 (Invitrogen) according to the manufacturer's instructions. Cells were lysed in lysis buffer containing 20 mM Tris (pH 7.5), 100 mM NaCl, 100 μM GDP, 5 mM $MgCl_2$, 1 mM EGTA, and 1% Triton X-100. To mimic the GTP hydrolysis transition state of the heterotrimeric G-protein α subunit, lysis buffer was supplemented with 20 mM NaF and 30 μM $AlCl_3$. Cell monolayers were scraped in lysis buffer and incubated at 4 °C for 45 min with sonication before insoluble components were separated by centrifugation at 14,000 × *g* at 4 °C for 10 min. Recombinant purified His_6-RGS21 protein (10 μg) was then added to the clarified cell lysate and rocked at 4 °C for 1 h before addition of NTA-agarose and continued incubation overnight at 4 °C with rocking. NTA-agarose was then washed four times with lysis buffer and bound proteins were resolved using SDS-PAGE electrophoresis, transferred to nitrocellulose, and detected by chemiluminescence using standard immunoblotting techniques.

Surface Plasmon Resonance (SPR) Assay

Optical detection of protein-protein interactions using SPR was performed using the Biacore 3000 (GE Healthcare) of University of North Carolina Center for Structure Biology exactly as previously described (57, 58).

Single-turnover GTPase Assay

The intrinsic and RGS protein-enhanced GTP hydrolysis rates of Gα subunits were assessed by monitoring the production of $^{32}P_i$ (inorganic phosphate) during a single round of [γ-^{32}P]GTP hydrolysis, as previously described (59). In brief, purified Gα subunits (100 nM) were separately incubated for 10 min at 20 °C with 1×10^6 cpm of [γ-^{32}P]GTP (PerkinElmer Life Science; specific activity of 6500 dpm/Ci) in reaction buffer lacking Mg^{2+} (50 mM Tris, pH 7.5, 0.05% (v/v) polyoxyethylene 10 laurel ether (C12E10), 1 mM DTT, 10 mM EDTA, 100 mM NaCl, and 5 μg/ml of BSA). The reaction was then chilled on ice for 5 min prior to initiation of the reaction by the addition of RGS protein, 10 mM $MgCl_2$, and 100 μM GTPγS (final concentration). At periodic intervals, 100-μl aliquots were quenched in 900 μl of charcoal slurry (*i.e.* 5% (w/v) activated charcoal in 50 mM H_3PO_4, pH 3.0) and centrifuged at 4 °C for 10 min at 3000 × *g*. Subsequently, 600-μl aliquots of the supernatant were counted via liquid scintillation to quantify $^{32}P_i$ production. Protocol modifications for quantifying GTPase activity from transducin were made as previously described (60).

Ex Vivo Tracheal Epithelial Cultures

Mouse tracheal epithelia (MTE) were obtained from *Rgs21*::RFP transgenic mice and aged-matched, wild-type C57Bl/6J mice by enzymatic digestion as previously described (61) under a protocol approved by the UNC IACUC. MTE were maintained at an air-liquid interface in a modified bronchial epithelial growth medium with 5% CO_2 at 37 °C and used 2–5 weeks after seeding on 12-mm T-clear inserts (Corning-Costar). To label the airway surface liquid, PBS containing 10-kDa FITC/dextran (0.2 mg/ml; Sigma) was added to MTE mucosal surfaces and then live MTE cultures were imaged by XZ confocal microscopy as previously described (62). Briefly, a 63X glycerol immersion objective was used; the airway surface liquid was imaged using a 488 nm argon laser and TagRFP protein was imaged using a 561 nm diode-pumped solid-state laser.

Stable shRNA-mediated Knockdown of Endogenous RGS21 Expression

Stable 16HBE cell lines with reduced RGS21 expression were generated via lentiviral infection. pLKO.1 plasmids encoding human *RGS21*-directed shRNA (Oligo IDs TRCN0000036859, TRCN0000036861, and TRCN0000036863; generated by The RNAi Consortium and purchased from Open Biosystems as catalogue number RHS3979–9604267, RHS3979–98492449, and RHS3979–9604271) were prepared from bacterial stocks via maxiprep (Qiagen; Valencia, CA) and packaged into lentiviral stocks by the UNC Lineberger Comprehensive Cancer Center Lenti-shRNA Core Facility (Dr. Tal Kafri, director). A control empty lentiviral vector (Open Biosystems catalogue number RHS4080) was also packaged to establish the negative control cell line. These viruses were used to infect separate 16HBE cell cultures seeded onto 100-mm dishes at 50% confluence. Stably transfected cell lines were selected with puromycin (Cellgro, Manassas, VA) and maintained in standard medium supplemented with puromycin for several weeks prior to use in second messenger assays.

siRNA Knockdown in 16HBE Cells

All siRNA used in this study were chemically synthesized by Dharmacon RNAi Technologies and purchased as an siGENOME set consisting of four individual siRNA oligonucleotide duplexes directed toward human *RGS21*. 16HBE cells seeded in 6-well plates were co-transfected with a pool of all four *RGS21*-directed siRNA oligonucleotide duplexes (100 nM) with Lipofectamine 2000 (Invitrogen) using the manufacturer's protocol. A control siRNA (siGlo Lamin A/C) was separately transfected to visualize transfection efficiency and act as a negative control. After 24 h, cells were seeded onto poly-D-lysine-

coated 96-well plates. Approximately 18–24 h after seeding, fluorescence imaging plate reader (FLIPR) assays for bitterant-induced calcium flux were performed as described above. Knockdown of the *RGS21* transcript was confirmed 48 h post-transfection via qRT-PCR.

FLIPR Calcium Flux Assays

Calcium flux assays were performed using the FLIPR^{TETRA} (Molecular Devices, Sunnyvale, CA) of the NIMH Psychoactive Drug Screening Program located at UNC (PDSP; Dr. Bryan Roth, director) as previously described (63). 16HBE cells were trypsinized, counted, and seeded onto clear-bottom 96-well plates (Greiner Bio-One, Monroe, NC) pre-coated with poly-D-lysine, at a density of 7.5×10^4 cells per well. After a 24-h incubation, media was removed and replaced with a no-wash dye (FLIPR® Calcium Assay Kit; Molecular Device Corp., Sunnyvale, CA). After a 1-h incubation at 37 °C, during which the cells were allowed to take up the dye, fluorescence responses of cells were measured with the FLIPR^{TETRA} device upon the addition of variable concentrations of tastant, or vehicle, in the presence of assay buffer (20 mM HEPES, pH 7.4, 1× Hanks' balanced salt solution (Invitrogen), and 2.5 mM probenecid). After 500 s of data acquisition, a subsequent addition of 5 μM thapsigargin or 3 M KCl was injected into each well, and fluorescence was measured again. Net peak responses to tastants were normalized to net peak responses to thapsigargin/KCl. Responses were compared with that of wild-type control 16HBE cells. Statistical and graphical analyses were performed using Prism version 5.0b (GraphPad Software, La Jolla, CA).

cAMP Accumulation GloSensor Assay

16HBE cell cultures were transiently co-transfected with the GloSensor cAMP-biosensor cDNA (Promega) and pcDNA3.1-based expression plasmids as previously described (64). Twenty-four hours post-transfection, cells were re-plated on poly-D-lysine-treated, clear-bottom, white 384-well plates at a density of 15,000 cells/well. Forty-eight hours post-transfection, culture medium was aspirated and cells were washed once with assay medium (DMEM (without FBS or phenol), 15 mM HEPES, pH 7.4) before being incubated for 2 h with 20 μl/well of equilibration medium (assay medium with 4% GloSensor^{TM} substrate (Promega)). After 2 h, 10 μl of 3× final concentration of denatonium benzoate (diluted in 3 mM forskolin-containing assay medium) was added to each well and allowed to incubate for 10 min before GloSensor emission was read on a MicroBeta Plate Counter (PerkinElmer). Before plotting, luminescence counts were normalized to 100% maximal response for each condition to account for variability in GloSensor expression, transfection efficiency, and the exact number of cells per well.

RESULTS AND DISCUSSION

RGS21 Is Expressed Outside of the Lingual Gustatory System—Given the discrepancy in expression patterns presented by the first two reports on RGS21 (47, 48), we profiled the expression of *Rgs21* transcripts by quantitative reverse transcription-PCR (qRT-PCR) on RNA isolated from various human as well as mouse tissues. In human tissues, *RGS21* was found highly expressed in circumvallate papillae and expressed at a lower level in lung tissue (Fig. 1*A*). This same pattern was also observed in mouse tissue, with the addition that *Rgs21* was also detected in RNA isolated from whole, homogenized mouse tongue (Fig. 1*C*). These results are consistent with the expression pattern of rat *Rgs21* originally described by von Buchholtz *et al.* (47). To identify more specifically the cellular distribution of mouse *Rgs21* expression within the lingual tissue, *in situ* hybridization was performed on sections of the mouse tongue. Using this approach, mouse *Rgs21* was detected in taste bud cells in the circumvallate papillae, with an expression pattern similar to those of *gustducin-α* and *PLCβ2* transcripts (Fig. 1, *E–G*).

Given recent evidence suggesting that gustation signaling components are expressed in enteroendocrine cells of the digestive tract (31, 32), we also analyzed *RGS21* transcript levels in different regions of the human and mouse gastrointestinal tract. Although *RGS21* transcripts were identified in various regions of the human gastrointestinal tract (Fig. 1*B*), *Rgs21* expression was not detectable in the mouse gastrointestinal tract (Fig. 1*D*). Although this may represent a difference in expression between the two organisms, it may also be the result of differential probe sensitivity; however, our results do suggest that *RGS21* expression is associated with tastant signaling components known to be expressed in gustatory cells of the human digestive tract (31, 32).

To explore further the expression pattern of the mouse *Rgs21* gene locus, a bacterial artificial chromosome (BAC) transgenic mouse strain was established that expresses TagRFP (50) driven by the *Rgs21* promoter. Consistent with the qRT-PCR data of Fig. 1*C* and *in situ* hybridization data of Fig. 1*G*, TagRFP protein was expressed in the taste buds of the circumvallate papillae (Fig. 2). In combining epifluorescence with immunofluorescence, TagRFP expression was found to be co-localized with gustducin α-subunit expression within taste bud cells (Fig. 2, *A–D*). To confirm the qRT-PCR data indicating *RGS21* expression in lung tissue, we cultured MTE cells from *Rgs21*::RFP transgenic mice at an air-liquid interface for 3 weeks; XZ confocal scanning revealed that TagRFP fluorescence was clearly detectable in MTE cells of transgenic mouse cultures, but undetectable in control mice (Fig. 2, *I–K*).

RGS21 Is Predicted to be a Highly Active, and Promiscuous, Gα-directed GAP—RGS21 belongs to the R4 family (9) of RGS proteins that are generally composed of little more than a central, ~130 amino acid RGS domain; indeed, at 152 amino acids long, RGS21 is mainly an RGS domain with short N- and C-terminal extensions. Some of us (65) recently described applying electrostatic calculations of interaction energies across multiple, high-resolution Gα/RGS protein structures (*e.g.* Refs. 66 and 67) to predict RGS domain residues essential for high-level GAP function and Gα substrate selectivity. Applying this energy-based, residue-level analysis to RGS21 (Fig. 3*A*) revealed that this RGS protein has the full complement of "significant and conserved" residues critical for the GAP activity of such highly active RGS proteins as RGS4 and RGS16. RGS21 also has eight "functional modulatory" residues (Fig. 3*A*), which is at the high end of the range (six to eight) observed in high activity RGS domains (65). Importantly, all of the RGS21 residues in modu-

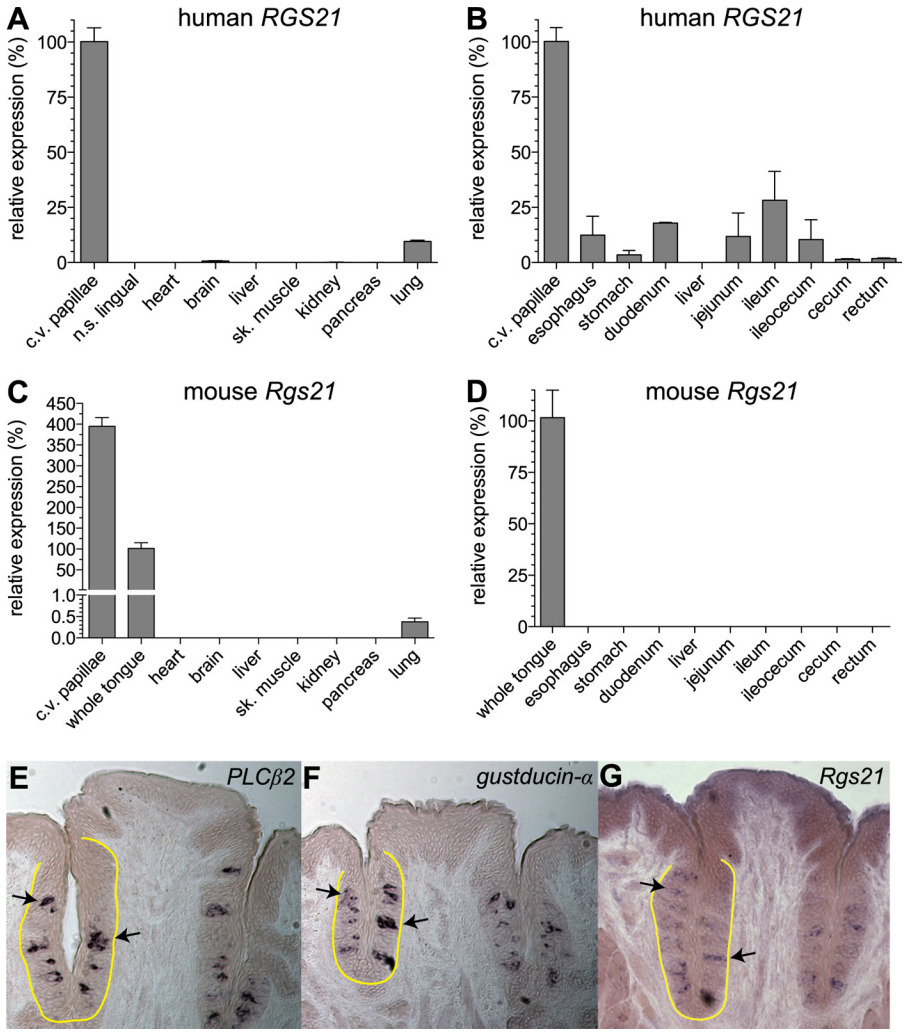

FIGURE 1. **RGS21 transcripts are highly expressed in lingual gustatory epithelium as well as in lung and human gastrointestinal tissues.** *A* and *B,* real-time, quantitative RT-PCR using fluorogenic probe detection was performed on total RNA from indicated human organs. Variable quantities of RNA were normalized by comparison to 18S ribosomal RNA and *RGS21* expression in the circumvallate (*c.v.*) papillae was set to "100% relative expression" using the $2^{-(\Delta\Delta Ct)}$ method (49). *C* and *D,* total RNA was extracted from the indicated mouse organs prior to quantitative RT-PCR analysis. Variation in total amounts of RNA isolated from each organ was normalized by comparison to 18S ribosomal RNA and *RGS21* expression in the whole tongue preparation was set to "100% relative expression" using the $2^{-(\Delta\Delta Ct)}$ method (49). *E--G*, coronal sections of mouse c.v. papillae were hybridized with digoxigenin riboprobes for *PLCβ2* (*E*), *gustducin-α* (aka *GNAT3*) (*F*), and *Rgs21* (*G*). Following hybridization and washes, probes were detected using an alkaline phosphatase-conjugated anti-digoxigenin antibody and 5-bromo-4-chloro-3-indolyl phosphate/nitro blue tetrazolium chromogenic development. Taste buds within stratified squamous epithelium along the left side of the depicted central c.v. papilla are outlined in *yellow*; examples of probe staining are indicated with *arrowheads*.

latory positions that are different from those in high activity RGS domains (four positions; Fig. 3*A*) were predicted not to interfere with canonical Gα recognition. Therefore, RGS21 was predicted to be a highly active and promiscuous Gα-directed GAP, similar to the high activity RGS domains that share the aforementioned structural properties (*e.g.* RGS4 and RGS16; Ref. 65).

RGS21 Interacts with Multiple Gα Subunits—Although R4-family RGS proteins, like RGS4 and RGS16, primarily bind to adenylyl cyclase inhibitory ($G\alpha_{i/o}$) and $G\alpha_{q/11}$ subunits (66–68), RGS proteins in general have also been reported to modulate signaling mediated through $G\alpha_s$ (69, 70), $G\alpha_{olf}$ (71), and $G\alpha_{12/13}$ (6, 72, 73) subunits. To identify the subset of Gα proteins that are capable of interacting with RGS21, pulldown assays were performed with recombinant His_6-RGS21 protein and cellular lysates containing overexpressed Gα subunits. RGS21 was observed to bind $G\alpha_{i1}$, $G\alpha_q$, rod and cone transducin-α (*GNAT1* and *GNAT2* gene products) and gustducin-α (*GNAT3*) in their transition state forms (*e.g.* bound with GDP/AlF_4^-) and not in their ground state, GDP-bound forms (Fig. 3*B*). These results with RGS21 are consistent with other reports that, with the exception of RGS2 (64, 74), all R4-family RGS domains can interact with both adenylyl cyclase inhibitory ($G_{i/o}$) and PLCβ stimulatory (G_q) Gα subunits (66, 75).

The primary Gα subunits implicated in gustation are gustducin-α and transducin-α (36–38). Based on the RGS9/transducin-α structure and its comparison to other RGS domain-Gα complexes (66, 76), the predicted RGS domain contact residues within gustducin-α are 95% identical and 100% similar to those of transducin-α (Fig. 3*C*). Given this degree of similarity, we expect that RGS21 acts equivalently on both transducin and gustducin-α subunits (the latter being far more difficult to obtain in purified form than transducin).

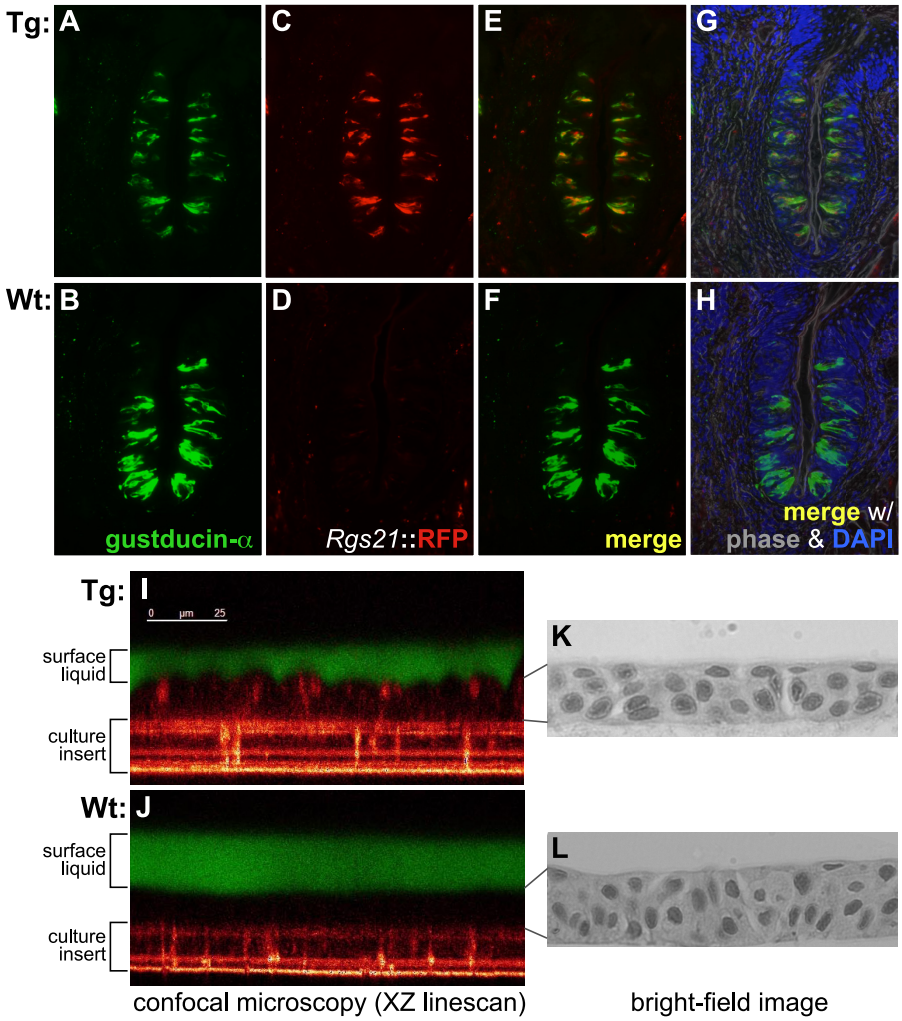

FIGURE 2. **The Rgs21 gene promoter is active in taste bud cells co-incident with gustducin-α expression, as well as in tracheal epithelium.** *A–G*, sections of mouse circumvallate papillae from *Rgs21*::RFP transgenic (*Tg*) and wild-type (*Wt*) mice were stained with anti-gustducin-α antibody and then imaged by epifluorescence to detect the expression pattern of gustducin-α (*green*; *panels A* and *B*) and TagRFP protein expressed from the *Rgs21* promoter (*red*; *panels C and D*). Images were merged, with co-localization of gustducin-α and RFP signals pseudocolored *yellow* (*panels E* and *F*) and additionally with phase-contrast and DNA staining (DAPI) colored *gray* and *blue*, respectively (*panels G* and *H*). *I–L*, explanted tracheal epithelium from *Rgs21*::RFP transgenic and wild-type mice was cultured *ex vivo* in an air-liquid interface for 3 weeks and then imaged for TagRFP protein expression by confocal microscopy (*panels I–J*) and for cellular morphology by bright-field microscopy (*panels K–L*). Air-liquid interface was highlighted by the addition of FITC-dextran to the airway surface liquid. Images presented are representative of $n = 6$ *Rgs21*::RFP transgenic and $n = 6$ wild-type mice were analyzed.

SPR spectroscopy was used to determine whether the RGS21/Gα interaction is direct and occurs in a manner consistent with the canonical RGS domain/Gα interaction (66, 67). An SPR biosensor surface was generated with either immobilized biotin-$G\alpha_{i1}$ or His_6-$G\alpha_q$ fusion protein, and RGS21 was subsequently injected over each surface, either in buffer containing aluminum tetrafluoride (to create the transition state form) or GDP alone. RGS21 bound selectively to $G\alpha_{i1}(GDP/AlF_4^-)$ and $G\alpha_q(GDP/AlF_4^-)$ with dissociation constants (K_d values) of 64 nM (95% confidence interval (CI) of 40 – 87 nM) and 20 nM (95% CI 11–29 nM), respectively (Fig. 4, *A* and *B*). These affinities for transition state Gα subunits are consistent with earlier reports from other R4-family RGS proteins obtained using SPR (77). No binding was observed to either $G\alpha_{i1}$ or $G\alpha_q$ surfaces when in their GDP-bound ground state. A charge reversal of the highly conserved Arg-126 (highlighted in Fig. 3*A*) to glutamic acid (R126E), previously shown to disrupt other RGS domain/Gα interactions (53, 64), was observed to disrupt the RGS21 interaction with $G\alpha_{i1}(GDP/AlF_4^-)$ and $G\alpha_q(GDP/AlF_4^-)$ surfaces. Circular dichroism studies were performed to verify that the global-fold of the mutant protein was preserved (Fig. 4*D*).

To verify the affinities observed with immobilized Gα biosensor surfaces, and to test additional purified Gα subunits for their interaction with RGS21, the SPR experimental setup was inverted (Fig. 4*C*) with a GST-RGS21 fusion protein biosensor surface being generated (57). Binding affinities (K_D values) for the interaction between GST-RGS21 and the GDP/AlF_4^--bound, transition state forms of $G\alpha_{i1}$, $G\alpha_{i2}$, $G\alpha_{i3}$, $G\alpha_o$, and transducin-α (Chi6 chimer; Ref. (55) were determined to be 114 (95% CI 65–163 nM), 63 (30 –95 nM), 61 (25–97 nM), 24 (18 –32 nM), and 190 nM (134 –247 nM), respectively; as previously observed (Fig. 4*B*), no binding was detected to GDP-bound Gα subunits (Fig. 4*C*).

RGS21 Is a Potent GAP for Multiple Gα Subunits in Vitro—To assess directly if RGS21 accelerates the GTPase activity of GTP-bound Gα subunits, RGS domain-mediated GAP activity

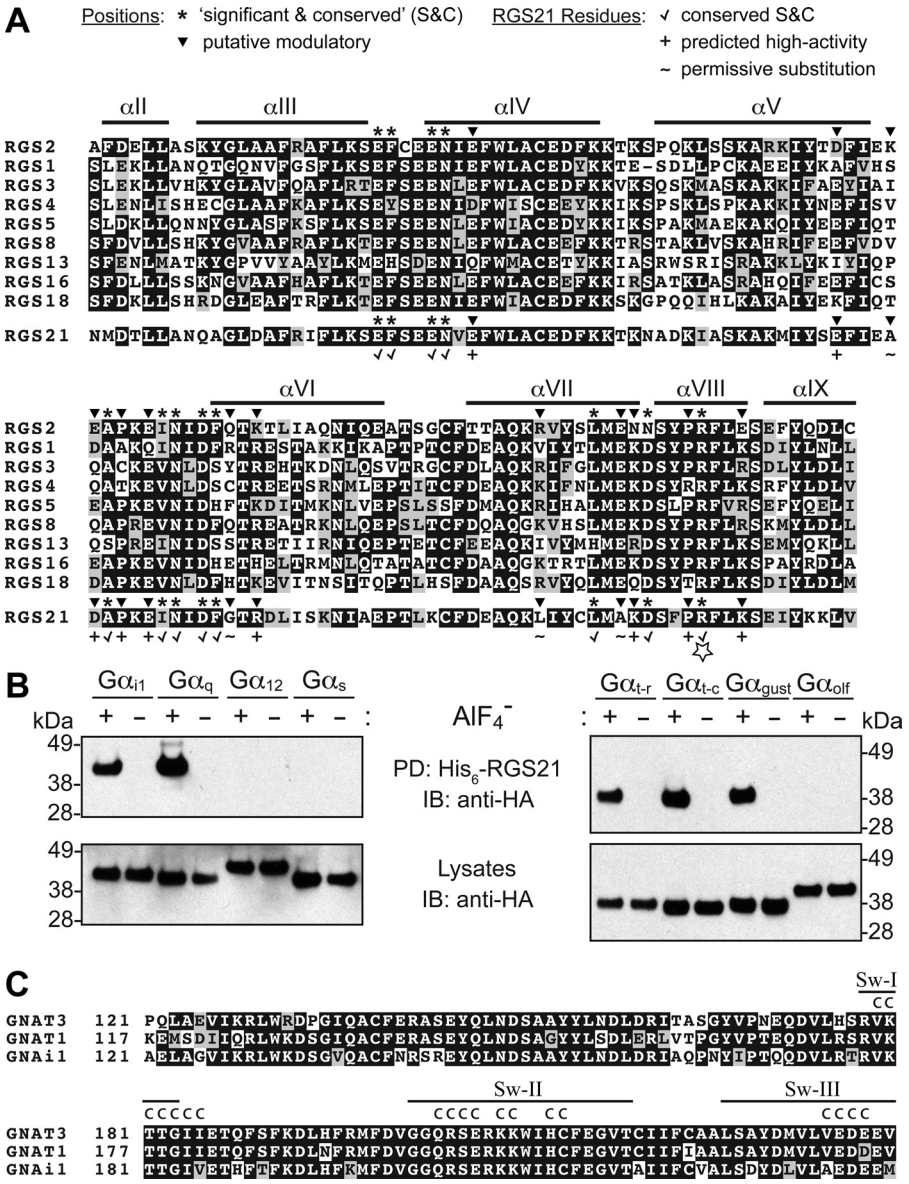

FIGURE 3. **Prediction and empirical examination of the Gα substrate promiscuity of RGS21.** *A,* multiple sequence alignment of the minimal RGS domain region of R4-family RGS proteins, highlighting regions of known α-helical secondary structure (*overlined*) and specific locations of significant and conserved and putative modulatory residue positions, as defined in Kosloff *et al.* (65). RGS21 residue arginine 126 is highlighted with an *open-star symbol*; this residue is known to be a highly conserved, surface-exposed constituent of the Gα-binding "A-site" of RGS domains. *B*, COS7 cells were transiently transfected with expression vectors for the indicated Gα subunits and, 48 h later, lysed in buffer containing GDP, Mg^{2+}, and AlF_4^- (+) or GDP only (−). Clarified cell lysates were incubated overnight at 4 °C with recombinant His_6-RGS21 protein and nickel-nitrilotriacetic acid-agarose beads (*PD,* pulldown), prior to detection of co-precipitated, HA-tagged Gα subunit by SDS-PAGE, electrotransfer to nitrocellulose, and immunoblotting (*IB*) with anti-HA antibody and chemiluminescence detection. *C*, gustducin and transducin Gα subunits have nearly identical interfaces for RGS domains. A protein sequence alignment of human gustducin-α (GNAT3, GenBank accession number NP_001095856.1), transducin-α (GNAT1, GenBank NP_653082.1), and $Gα_{i1}$ (GNAi1, GenBank NP_002060.4) was generated using ClustalW. Contacts between the Ras-like domain of transducin-α (Chain A) and the RGS9 RGS domain (Chain B) from the RGS9/transducin-α structure (PDB code 1FQK; Ref. 76) were identified using contact map analysis (83) and are denoted with a *C above* the alignment. *Sw*, switch region.

was measured using a single round of [γ-^{32}P]GTP hydrolysis, commonly referred to as "single turnover" assays (59, 78). RGS21 robustly accelerated the hydrolysis of GTP by $Gα_{i1}$ (Fig. 5*A*): the intrinsic GTPase rate by 100 nM $Gα_{i1}$ was determined to be 0.009 s^{-1} (95% CI 0.007–0.011 s^{-1}), whereas the GTPase rate upon addition of a substoichiometric amount of RGS21 (50 nM) was 0.25 s^{-1} (95% CI 0.11–0.38 s^{-1}), over 25 times faster. RGS21-mediated GAP activity was also observed using recombinant $Gα_{i2}$, $Gα_{i3}$, and $Gα_o$, as well as transducin-α purified from bovine rod outer segments (Fig. 5, *C–F*; summarized in Table 1).

To ensure that these observed hydrolysis rate increases were not due to contaminating GTPase(s) in the RGS21 protein preparation, single turnover assays were repeated with a RGS-insensitive $Gα_{i1}$ point mutant, $Gα_{i1}$(G183S) (79). The intrinsic hydrolysis rate of $Gα_{i1}$(G183S) was not accelerated upon the addition of 250 nM of either wild-type RGS21 or RGS21(R126E) proteins (Fig. 5*B*).

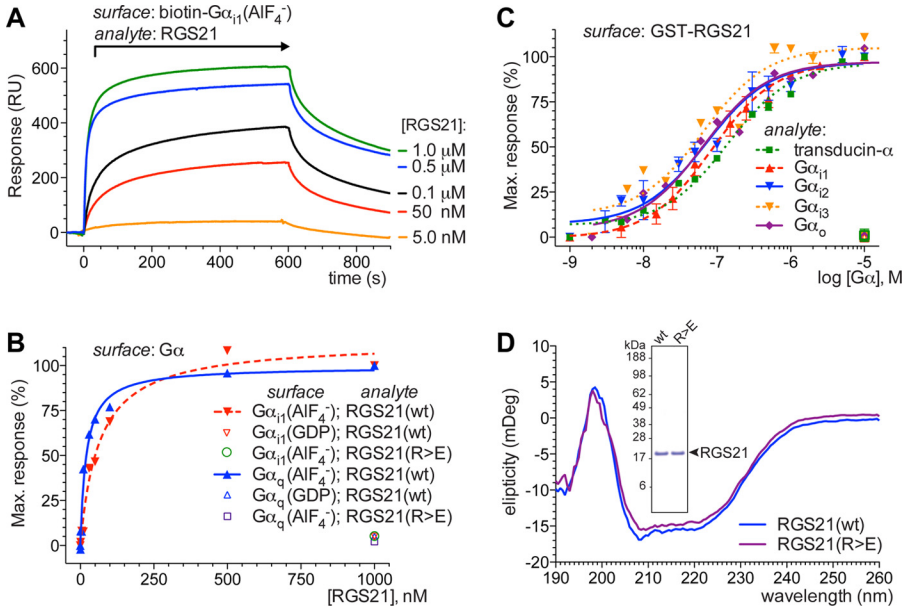

FIGURE 4. **RGS21 interacts with transition-state forms of $G\alpha_q$ and $G\alpha_{i/o}$ subunits with nanomolar affinities.** *A*, biotin-$G\alpha_{i1}$ and alkaline-denatured biotin-$G\alpha_{i1}$ were immobilized on separate streptavidin biosensor surfaces for SPR binding analyses. Indicated concentrations of recombinant RGS21 protein were injected over both surfaces at 20 μl/min for 600 s (injection start at $t = 0$) with a subsequent 300-s dissociation time. Nonspecific binding to the alkaline-denatured biotin-$G\alpha_{i1}$ surface was subtracted using BiaEvaluation software. *B*, sensorgrams derived from experiments as illustrated in *panel A* were used for equilibrium saturation binding analyses to determine the affinity of wild-type RGS21 or RGS21(R126E) proteins for $G\alpha_{i1}$ or $G\alpha_q$ in both their transition state (GDP/AlF_4^-) and ground state forms. $G\alpha_q$ biosensor sensorgrams were obtained by immobilizing His_6-$G\alpha_q$ using capture coupling. Dissociation constants (K_D values) for the $G\alpha_{i1}(GDP/AlF_4^-)$/RGS21 and $G\alpha_q(GDP/AlF_4^-)$/RGS21 interactions were determined to be 64 (95% CI 40–87 nM) and 20 nM (95% CI 11–29 nM), respectively. No specific binding was observed for the loss-of-function RGS21(R126E) protein toward $G\alpha_{i1}$ or $G\alpha_q$ nor for wild-type RGS21 toward GDP-bound $G\alpha_{i1}$ or $G\alpha_q$. *C*, GST-RGS21 fusion protein or GST alone was immobilized on an anti-GST antibody biosensor surface. 200 μl of the indicated concentrations of various $G\alpha$ subunits (in their transition state form) were injected over the biosensor surface. Nonspecific binding toward GST alone was subtracted using BiaEvaluation. The binding at $t = 590$ s was plotted and used for equilibrium binding analyses. The affinities of $G\alpha_{i1}$, $G\alpha_{i2}$, $G\alpha_{i3}$, $G\alpha_o$, and transducin-α for immobilized RGS21 were determined to be 114 (95% CI 65–163 nM), 63 (30–95 nM), 61 (25–97 nM), 24 (18–32 nM), and 190 nM (134–247 nM), respectively. *Open symbols* denote no binding was detected when the various $G\alpha$ subunits were in their ground state, GDP-loaded form. *D*, wild-type RGS21 and RGS21(R126E) proteins were observed to have similar overall secondary structure by circular dichroism analysis. Circular dichroism spectra were separately collected using 0.1 mg/ml of RGS21 and RGS21(R126E) proteins. Spectra were collected from 185 to 260 nm in 0.5-nm steps with a bandwidth of 2 nm. *Inset*, RGS21 proteins used in these biochemical analyses were equivalently purified from *E. coli* fermentation, as highlighted by Coomassie Blue staining after being resolved by SDS-PAGE.

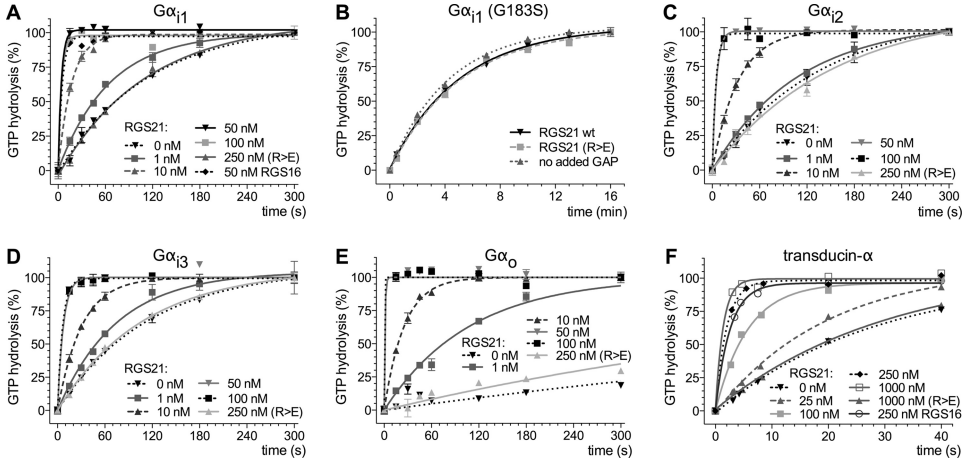

FIGURE 5. **RGS21 acts as a GAP for $G_{i/o}$ subfamily $G\alpha$ subunits.** Intrinsic GTPase activity of the indicated $G\alpha$ subunits, as well as RGS protein acceleration of this activity, was determined using [γ-^{32}P]GTP single turnover assays. In the absence of Mg^{2+}, 100 nM $G\alpha_{i1}$ (*A*), RGS-insensitive $G\alpha_{i1}$(G183S) (*B*), $G\alpha_{i2}$ (*C*), $G\alpha_{i3}$ (*D*), and $G\alpha_{oA}$ (*E*) were preincubated with [γ-^{32}P]GTP at 30 °C for 10 min. The reaction was then initiated by the addition of $MgCl_2$ (10 mM), the indicated concentrations of recombinant RGS protein, and cold GTPγS (400 μM). At the indicated time points, the production of inorganic phosphate was quantified by activated charcoal filtration and subsequent liquid scintillation. *F*, assays of transducin GTPase activity were conducted on a preformed complex between the G-protein heterotrimer (transducin-$\alpha\beta\gamma$; 2 μM) and the photoreceptor rhodopsin (20 μM) and were initiated by addition of [γ-^{32}P]GTP supplemented with GTP (250 nM). Nonlinear regression was used to fit the data to a single exponential function; observed rates are presented in Table 1.

RGS21 Overexpression Blunts Bitter Tastant Responsiveness of a Human Lung Airway Epithelial Cell Line—To determine whether RGS21 is capable of modulating gustatory signaling in an integrated, whole cell context, we first used RT-PCR to identify a model cell line expressing components of the gustatory signaling cascade as well as endogenous *RGS21*. The transformed human bronchial epithelial cell line 16HBE (80) was found to express mRNA transcripts for *RGS21*, multiple tastant

TABLE 1

Concentration dependence of RGS21-mediated acceleration of Gα GTP hydrolysis rates as observed in single turnover assays

Rates were determined using nonlinear regression of data obtained at 4 °C (Fig. 5) using Prism 5.0 and are expressed in s^{-1}. 95% confidence intervals are shown in parentheses. The empty cell indicates that the rate was not determined.

RGS21 (nM)	$G\alpha_{i1}$	$G\alpha_{i1}$ (G183S)	$G\alpha_{i2}$	$G\alpha_{i3}$	$G\alpha_{o}$	Transducin-α
0	0.0090 (0.0071–0.011)	0.0039 (0.0036–0.0042)	0.0074 (0.0058–0.0091)	0.0088 (0.0079–0.0097)	0.00082 (0.00052–0.0011)	0.036 (0.020–0.051)
1	0.015 (0.013–0.018)		0.0092 (0.0081–0.010)	0.013 (0.010–0.016)	0.0092 (0.0083–0.010)	
10	0.060 (0.051–0.068)		0.031 (0.028–0.034)	0.033 (0.030–0.036)	0.039 (0.037–0.042)	
25						0.051 (0.034–0.067)
50	0.25 (0.11–0.38)		0.20 (0.14–0.25)	0.14 (0.10–0.17)	NC[a]	
100	0.23 (0.078–0.38)		0.22 (0.065–0.37)	0.16 (0.12–0.19)	NC	0.18 (0.12–0.23)
250		0.0033 (0.0029–0.0036)				0.51 (0.35–0.67)
250; R126E	0.0090 (0.0071–0.011)	0.0033 (0.0029–0.0037)	0.0065 (0.0048–0.0082)	0.0093 (0.0084–0.010)	0.0014 (0.0012–0.0017)	
1000						0.74 (0.25–1.2)
1000; R126E						0.033 (0.013–0.053)

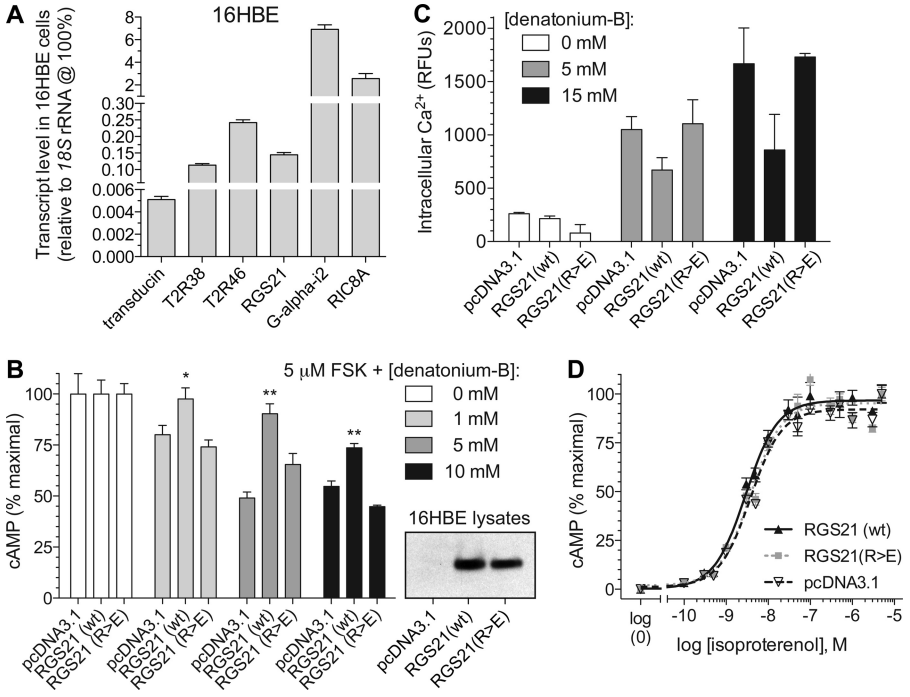

FIGURE 6. **Overexpression of wild-type RGS21, but not a loss-of-function, point mutant, leads to reduction of bitter tastant signaling.** *A,* real-time qRT-PCR using fluorogenic probe detection was performed on total RNA from the human bronchial epithelium cell line 16HBE to detect the indicated gene transcripts; data were normalized to levels of *18S* rRNA detection. *B,* 16HBE cell cultures were transiently co-transfected with the Promega GloSensor cAMP-biosensor cDNA and expression plasmids containing HA epitope-tagged open reading frames for wild-type (wt) rat RGS21, or Arg-126 to Glu point mutated (Arg → Glu) rat RGS21, or empty pcDNA3.1 vector, as indicated. Inhibition of forskolin (*FSK*) stimulated cAMP production by treatment with the indicated concentrations of denatonium-B was determined 24 h post-transfection by detection of GloSensor-dependent luminescence. *Inset*, Western blot of whole cell lysates from transfected 16HBE cultures with anti-HA-epitope antibody and chemiluminescence detection, demonstrating equivalent expression of wild-type and point mutant RGS21 proteins. *Asterisks* denote statistically significant differences from signal obtained upon empty vector expression: *, $p < 0.05$; **, $p < 0.01$ (one-way analysis of variance with Bonferroni's post-test). *C,* 16HBE cell cultures were transiently transfected with expression plasmids containing wild-type (*wt*) RGS21, or point mutated (Arg → Glu) RGS21, or empty vector, as indicated. Net peak intracellular calcium production, as elicited by treatment with the indicated concentrations of denatonium-B was determined using calcium indicator dye and fluorometric imaging plate reader (FLIPR) detection (relative fluorescence units, *RFU*), 48 h post-transfection. *D,* isoproterenol-stimulated production of cAMP is not perturbed by overexpression of RGS21 or RGS21(R126E) in 16HBE cells. Cells were transfected exactly as described in *panel B*. Isoproterenol-induced cAMP production was detected by GloSensor-dependent luminescence. EC_{50} values for isoproterenol were found to be 2.9 (95% CI 2.3–3.7 nM), 3.8 (3.1–4.7 nM), and 3.8 nM (3.1–4.7 nM) for 16HBE cells overexpressing wild-type RGS21, RGS21(R126E), and empty vector, respectively.

receptors (*e.g.* the bitter tastant receptors T2R38 and T2R46), and downstream components of the tastant signaling pathway (Fig. 6*A*).

Bitter tastant signaling is known to rapidly reduce cellular cyclic nucleotide levels (40). To test the hypothesis that RGS21 can serve as a negative regulator of bitter tastant signal transduction, the bitter receptor agonist denatonium benzoate ("denatonium-B") was applied to 16HBE cells and the resultant cAMP decreases were monitored in the context of artificially heightened cAMP levels (*i.e.* forskolin-mediated activation of endogenous adenylyl cyclases). In a concentration-dependent fashion (Fig. 6*B*), denatonium-B application reduced forskolin-mediated cAMP production, as predicted (40); overexpression of wild-type RGS21, but not the GAP-dead RGS21(R126E) mutant, significantly blunted the bitter tastant-induced reduction in cAMP production. To ensure that RGS21 overexpression did not have unanticipated, global consequences on GPCR-mediated signaling, isoproterenol-activated production of cAMP (via β-adrenergic receptor activation) was also monitored in 16HBE cells overexpressing wild-type RGS21, RGS21(R126E), or vector alone. No significant alteration in the potency (EC_{50} values) of isoproterenol upon RGS21 overexpression was observed (Fig. 6*D*).

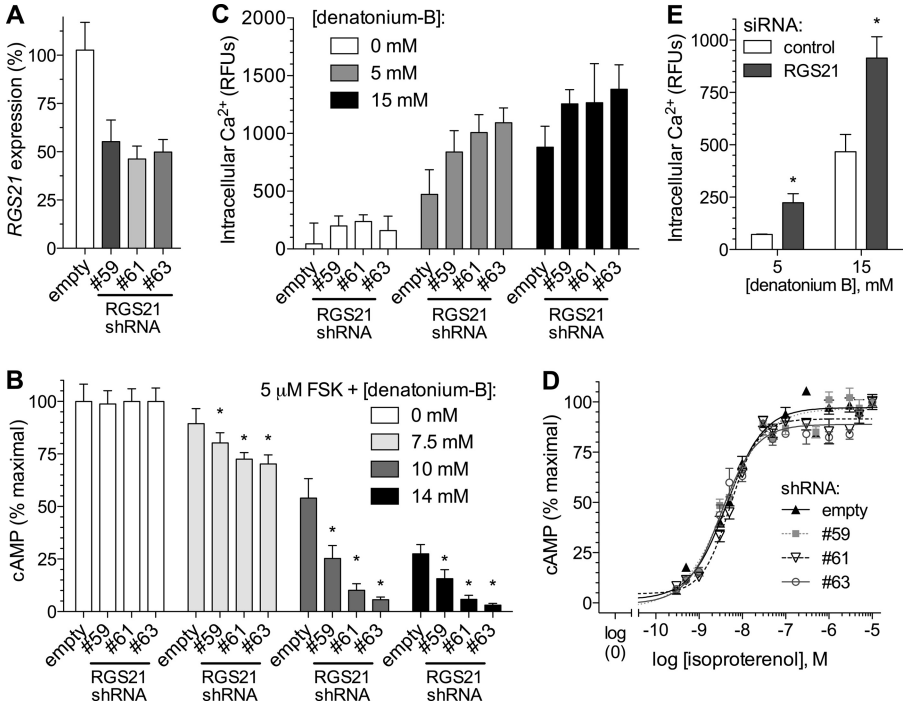

FIGURE 7. **RNA interference-mediated knockdown of endogenous RGS21 potentiates bitter tastant signaling.** *A*, quantitative RT-PCR demonstrating shRNA-mediated knockdown of *RGS21* transcript levels in stable, lentivirus-transfected variants of the human bronchial epithelial cell line 16HBE. Real-time, quantitative PCR using fluorogenic probe detection was performed for the *RGS21* transcript, normalized to *18S* rRNA signal, and expressed as the percentage of *RGS21* expression observed in control 16HBE cells stably transfected with empty lentivirus. *B*, 16HBE cells were stably transfected with either empty lentivirus (*Empty*) or one of three, *RGS21*-directed shRNA-expressing lentiviruses (*#59*, *#61*, *#63*), as indicated. Inhibition of forskolin-stimulated cAMP production by treatment with the indicated concentrations of denatonium-B were determined 24 h post-transfection by detection of GloSensor-dependent luminescence. *Asterisks* denote statistically significant differences from empty vector, $p < 0.01$ (one-way analysis of variance with Dunnett's multiple comparison test). *C*, net peak intracellular calcium production by 16HBE cells stably expressing the indicated lentiviruses, as elicited by treatment with the indicated concentrations of denatonium-B, was determined using calcium indicator dye and FLIPR detection (relative fluorescence units, *RFU*). *D*, isoproterenol-stimulated cAMP production is not perturbed by shRNA-mediated *RGS21* knockdown. Cells were treated exactly as described in *panel B*. Isoproterenol-induced cAMP production was detected by GloSensor-dependent luminescence. EC_{50} values for isoproterenol were 4.4 (95% CI 3.6–5.5 nM), 3.7 2.9–4.8 nM), 5.2 (4.4–6.1 nM), and 3.2 nM (2.4–4.1 nM) for 16HBE cells expressing empty vector control, shRNA#59, shRNA#61, or shRNA#63, respectively. *E*, parental 16HBE cells were transfected with nonspecific (*Control*) or RGS21-directed short-interfering RNA oligonucleotide duplexes (siRNA), prior to measurement of denatonium-B-stimulated calcium flux as in *panel C*. *, $p < 0.03$ (unpaired Student's *t* test).

In tastant receptor signal transduction, the released $G\beta\gamma$ heterodimer is thought to play a key role in intracellular signaling via PLC-β2 activation (18, 42), which results in production of IP_3 and DAG second messengers and a subsequent increase in intracellular calcium (81). To determine whether RGS21 is also able to inhibit tastant-mediated activation of Ca^{2+} release, we monitored intracellular calcium in 16HBE cells upon denatonium-B treatment. A decrease in the intracellular Ca^{2+} flux caused by treatment with denatonium-B was observed in RGS21-overexpressing 16HBE cells, as compared with cells overexpressing the GAP-dead RGS21(R126E) mutant or transfected with empty vector only (Fig. 6*C*).

Knockdown of Endogenous RGS21 Expression Enhances Bitter Tastant Responsiveness—Although both cAMP accumulation and Ca^{2+} mobilization data suggest that RGS21 can act as a negative regulator of bitter tastant signaling upon its ectopic overexpression, we also wanted to test whether endogenous RGS21 expression serves to negatively regulate denatonium-B signaling. Three stable 16HBE cell lines were generated with decreased *RGS21* expression using lentiviral shRNA-mediated knockdown (Fig. 7*A*). No difference was seen in levels of forskolin-stimulated cAMP production in the absence of denatonium-B; however, upon denatonium-B treatment, significant decreases in cAMP generation were observed in all three cell lines with reduced *RGS21* expression *versus* the control lentivirus-treated cell line (Fig. 7*B*). To confirm that stable *RGS21* knockdown had not disrupted GPCR-mediated cAMP signaling in a nonspecific fashion, isoproterenol responses were also tested in these cell lines. No significant different in potency or maximal efficacy of isoproterenol was observed (Fig. 7*D*). Intracellular Ca^{2+} flux responses were also measured in the stable shRNA-mediated knockdown cell lines upon denatonium-B addition. At both agonist concentrations tested, decreased *RGS21* expression resulted in an increase in denatonium-B-induced intracellular Ca^{2+} accumulation (Fig. 7*C*). Increased calcium flux upon denatonium-B treatment was also observed upon siRNA-mediated knockdown of *RGS21* expression (Fig. 7*E*).

Conclusions—RGS21 is capable of interacting with, and serving as a GAP for, multiple G protein α subunits, including those thought to be involved in gustatory signal transduction. *RGS21* is endogenously expressed in human and mouse lingual and airway epithelia and human intestinal tissues. The observed tissue expression pattern of *RGS21* lies between those reported in two previous studies (47, 48): whereas *RGS21* is clearly expressed in lingual taste bud cells (47), it is also expressed in other tissues with gustatory epithelia. Interestingly, all of these tissues additionally express tastant receptors and other, down-

stream components of the gustatory signaling cascade (31–34), suggesting a role for RGS21 in negatively regulating tastant signal transduction in multiple cell types.

In identifying a human airway epithelial cell line (16HBE) that co-expresses RGS21, bitter tastant receptors, and downstream tastant signaling proteins, we have established that RGS21 indeed serves to blunt intracellular signaling by at least one tastant agonist, namely the bitterant denatonium. As lingual epithelium-derived taste bud cells are notoriously difficult to maintain in culture (82), our results suggest that established, immortalized lung epithelial cells may present a useful alternative system in which to study the action of RGS21 and other modulatory molecules on gustatory signal transduction using endogenous machinery (*e.g.* avoiding receptor and/or effector overexpression); however, it is possible that the signaling cascade in airway cells is different from that in taste bud cells because of differing subcellular environments and/or downstream effectors. In the taste bud, it is likely that RGS21 and/or other RGS proteins help to dampen signaling so that the gustatory system is not overwhelmed when molecules are abundant on the lingual epithelium. In the airway, detection of bitter tastants is hypothesized to help with mucus clearance of irritants by increasing cilia beat frequency (33, 34); thus, the role of RGS21 in lung epithelium may be to regulate mucus clearance by cillated airway cells in response to bitter irritants.

Acknowledgments—We thank Dr. Hyung-Suk Kim (Gene Expression Core, University of North Carolina) for assisting with RT-PCR assays, Dr. Megumi Aita (In situ Hybridization Core, University of North Carolina Neuroscience Center) for assistance with in situ hybridization, Drs. Bryan Roth and X. P. Huang for FLIPR access and advice, Dr. Dale Cowley of the University of North Carolina Animal Models Core for assistance with transgenic mouse strain creation, and Kimberlie Burns (Cystic Fibrosis Center Histology Core, University of North Carolina) for histological advice.

REFERENCES

1. Jacoby, E., Bouhelal, R., Gerspacher, M., and Seuwen, K. (2006) The 7 TM G-protein-coupled receptor target family. *Chem. Med. Chem.* **1,** 761–782
2. Mombaerts, P. (1999) Seven-transmembrane proteins as odorant and chemosensory receptors. *Science* **286,** 707–711
3. Lefkowitz, R. J. (2007) Seven transmembrane receptors. Something old, something new. *Acta Physiol.* **190,** 9–19
4. Bourne, H. R. (1997) How receptors talk to trimeric G proteins. *Curr. Opin. Cell Biol.* **9,** 134–142
5. Sprang, S. (1997) G protein mechanisms. Insight from structural analysis. *Annu. Rev. Biochem.* **66,** 639–678
6. Kozasa, T., Jiang, X., Hart, M. J., Sternweis, P. M., Singer, W. D., Gilman, A. G., Bollag, G., and Sternweis, P. C. (1998) p115 RhoGEF, a GTPase activating protein for $G\alpha_{12}$ and $G\alpha_{13}$. *Science* **280,** 2109–2111
7. Ford, C. E., Skiba, N. P., Bae, H., Daaka, Y., Reuveny, E., Shekter, L. R., Rosal, R., Weng, G., Yang, C. S., Iyengar, R., Miller, R. J., Jan, L. Y., Lefkowitz, R. J., and Hamm, H. E. (1998) Molecular basis for interactions of G protein betagamma subunits with effectors. *Science* **280,** 1271–1274
8. Dascal, N. (2001) Ion-channel regulation by G proteins. *Trends Endocrinol. Metab.* **12,** 391–398
9. Ross, E. M., and Wilkie, T. M. (2000) GTPase-activating proteins for heterotrimeric G proteins. Regulators of G protein signaling (RGS) and RGS-like proteins. *Annu. Rev. Biochem.* **69,** 795–827
10. Arshavsky, V. Y., and Pugh, E. N., Jr. (1998) Lifetime regulation of G protein-effector complex. Emerging importance of RGS proteins. *Neuron* **20,** 11–14
11. De Vries, L., Zheng, B., Fischer, T., Elenko, E., and Farquhar, M. G. (2000) The regulator of G protein signaling family. *Annu. Rev. Pharmacol. Toxicol.* **40,** 235–271
12. Druey, K. M., Blumer, K. J., Kang, V. H., and Kehrl, J. H. (1996) Inhibition of G-protein-mediated MAP kinase activation by a new mammalian gene family. *Nature* **379,** 742–746
13. Koelle, M. R., and Horvitz, H. R. (1996) EGL-10 regulates G protein signaling in the C. elegans nervous system and shares a conserved domain with many mammalian proteins. *Cell* **84,** 115–125
14. Siderovski, D. P., Hessel, A., Chung, S., Mak, T. W., and Tyers, M. (1996) A new family of regulators of G-protein-coupled receptors? *Curr. Biol.* **6,** 211–212
15. Lambert, N. A., Johnston, C. A., Cappell, S. D., Kuravi, S., Kimple, A. J., Willard, F. S., and Siderovski, D. P. (2010) Regulators of G-protein signaling accelerate GPCR signaling kinetics and govern sensitivity solely by accelerating GTPase activity. *Proc. Natl. Acad. Sci. U.S.A.* **107,** 7066–7071
16. Chen, C. K., Burns, M. E., He, W., Wensel, T. G., Baylor, D. A., and Simon, M. I. (2000) Slowed recovery of rod photoresponse in mice lacking the GTPase accelerating protein RGS9–1. *Nature* **403,** 557–560
17. Arshavsky, V. Y., Lamb, T. D., and Pugh, E. N., Jr. (2002) G proteins and phototransduction. *Annu. Rev. Physiol.* **64,** 153–187
18. Chandrashekar, J., Hoon, M. A., Ryba, N. J., and Zuker, C. S. (2006) The receptors and cells for mammalian taste. *Nature* **444,** 288–294
19. Meyerhof, W. (2005) Elucidation of mammalian bitter taste. *Rev. Physiol. Biochem. Pharmacol.* **154,** 37–72
20. Mueller, K. L., Hoon, M. A., Erlenbach, I., Chandrashekar, J., Zuker, C. S., and Ryba, N. J. (2005) The receptors and coding logic for bitter taste. *Nature* **434,** 225–229
21. Li, X., Staszewski, L., Xu, H., Durick, K., Zoller, M., and Adler, E. (2002) Human receptors for sweet and umami taste. *Proc. Natl. Acad. Sci. U.S.A.* **99,** 4692–4696
22. Nelson, G., Chandrashekar, J., Hoon, M. A., Feng, L., Zhao, G., Ryba, N. J., and Zuker, C. S. (2002) An amino acid taste receptor. *Nature* **416,** 199–202
23. Lockhart, I. A., Mitchell, S. A., and Kelly, S. (2009) Safety and tolerability of donepezil, rivastigmine and galantamine for patients with Alzheimer's disease. Systematic review of the "real-world" evidence. *Dement Geriatr Cogn Disord* **28,** 389–403
24. Matsui, D. (2007) Current issues in pediatric medication adherence. *Paediatr. Drugs* **9,** 283–288
25. Mennella, J. A., and Beauchamp, G. K. (2008) Optimizing oral medications for children. *Clin. Ther.* **30,** 2120–2132
26. Renwick, W., Pettengell, R., and Green, M. (2009) Use of filgrastim and pegfilgrastim to support delivery of chemotherapy. Twenty years of clinical experience. *BioDrugs* **23,** 175–186
27. Saito, M., Hoshi, M., Igarashi, A., Ogata, H., and Edo, K. (1999) The marked inhibition of the bitter taste of polymyxin B sulfate and trimethoprim X sulfamethoxazole by flavored BMI-60 in pediatric patients. *Biol. Pharm. Bull* **22,** 997–998
28. Shah, P. P., and Mashru, R. C. (2010) Palatable reconstitutable dry suspension of artemether for flexible pediatric dosing using cyclodextrin inclusion complexation. *Pharm. Dev. Technol.* **15,** 276–285
29. Horne, J., Lawless, H. T., Speirs, W., and Sposato, D. (2002) Bitter taste of saccharin and acesulfame-K. *Chem. Senses* **27,** 31–38
30. Kuhn, C., Bufe, B., Winnig, M., Hofmann, T., Frank, O., Behrens, M., Lewtschenko, T., Slack, J. P., Ward, C. D., and Meyerhof, W. (2004) Bitter taste receptors for saccharin and acesulfame K. *J. Neurosci.* **24,** 10260–10265
31. Wu, S. V., Chen, M. C., and Rozengurt, E. (2005) Genomic organization, expression, and function of bitter taste receptors (T2R) in mouse and rat. *Physiol. Genomics* **22,** 139–149
32. Wu, S. V., Rozengurt, N., Yang, M., Young, S. H., Sinnett-Smith, J., and Rozengurt, E. (2002) Expression of bitter taste receptors of the T2R family in the gastrointestinal tract and enteroendocrine STC-1 cells. *Proc. Natl. Acad. Sci. U.S.A.* **99,** 2392–2397
33. Kinnamon, S. C. (2012) Taste receptor signalling. From tongues to lungs. *Acta Physiol.* **204,** 158–168

34. Shah, A. S., Ben-Shahar, Y., Moninger, T. O., Kline, J. N., and Welsh, M. J. (2009) Motile cilia of human airway epithelia are chemosensory. *Science* **325,** 1131–1134
35. McLaughlin, S. K., McKinnon, P. J., and Margolskee, R. F. (1992) Gustducin is a taste-cell-specific G protein closely related to the transducins. *Nature* **357,** 563–569
36. Wong, G. T., Gannon, K. S., and Margolskee, R. F. (1996) Transduction of bitter and sweet taste by gustducin. *Nature* **381,** 796–800
37. He, W., Yasumatsu, K., Varadarajan, V., Yamada, A., Lem, J., Ninomiya, Y., Margolskee, R. F., and Damak, S. (2004) Umami taste responses are mediated by β-transducin and α-gustducin. *J. Neurosci.* **24,** 7674–7680
38. Kusakabe, Y., Yasuoka, A., Asano-Miyoshi, M., Iwabuchi, K., Matsumoto, I., Arai, S., Emori, Y., and Abe, K. (2000) Comprehensive study on G protein α-subunits in taste bud cells, with special reference to the occurrence of $G\alpha_{i2}$ as a major Gα species. *Chem. Senses* **25,** 525–531
39. Ueda, T., Ugawa, S., Yamamura, H., Imaizumi, Y., and Shimada, S. (2003) Functional interaction between T2R taste receptors and G-protein α subunits expressed in taste receptor cells. *J. Neurosci.* **23,** 7376–7380
40. Yan, W., Sunavala, G., Rosenzweig, S., Dasso, M., Brand, J. G., and Spielman, A. I. (2001) Bitter taste transduced by PLC-β_2-dependent rise in IP_3 and α-gustducin-dependent fall in cyclic nucleotides. *Am. J. Physiol. Cell Physiol.* **280,** C742–751
41. Damak, S., Rong, M., Yasumatsu, K., Kokrashvili, Z., Pérez, C. A., Shigemura, N., Yoshida, R., Mosinger, B., Jr., Glendinning, J. I., Ninomiya, Y., and Margolskee, R. F. (2006) Trpm5 null mice respond to bitter, sweet, and umami compounds. *Chem. Senses* **31,** 253–264
42. Zhang, Y., Hoon, M. A., Chandrashekar, J., Mueller, K. L., Cook, B., Wu, D., Zuker, C. S., and Ryba, N. J. (2003) Coding of sweet, bitter, and umami tastes. Different receptor cells sharing similar signaling pathways. *Cell* **112,** 293–301
43. Reiter, E., and Lefkowitz, R. J. (2006) GRKs and β-arrestins. Roles in receptor silencing, trafficking and signaling. *Trends Endocrinol Metab.* **17,** 159–165
44. Kimple, A. J., Bosch, D. E., Giguère, P. M., and Siderovski, D. P. (2011) Regulators of G-protein signaling and their Gα substrates. Promises and challenges in their use as drug discovery targets. *Pharmacol. Rev.* **63,** 728–749
45. Behrens, M., Bartelt, J., Reichling, C., Winnig, M., Kuhn, C., and Meyerhof, W. (2006) Members of RTP and REEP gene families influence functional bitter taste receptor expression. *J. Biol. Chem.* **281,** 20650–20659
46. Fenech, C., Patrikainen, L., Kerr, D. S., Grall, S., Liu, Z., Laugerette, F., Malnic, B., and Montmayeur, J. P. (2009) Ric-8A, a Gα protein guanine nucleotide exchange factor potentiates taste receptor signaling. *Front. Cell Neurosci.* **3,** 11
47. von Buchholtz, L., Elischer, A., Tareilus, E., Gouka, R., Kaiser, C., Breer, H., and Conzelmann, S. (2004) RGS21 is a novel regulator of G protein signalling selectively expressed in subpopulations of taste bud cells. *Eur. J. Neurosci.* **19,** 1535–1544
48. Li, X., Chen, L., Ji, C., Liu, B., Gu, J., Xu, J., Zou, X., Gu, S., and Mao, Y. (2005) Isolation and expression pattern of *RGS21* gene, a novel RGS member. *Acta Biochim. Pol.* **52,** 943–946
49. Livak, K. J., and Schmittgen, T. D. (2001) Analysis of relative gene expression data using real-time quantitative PCR and the $2(-\Delta\Delta C_T)$ method. *Methods* **25,** 402–408
50. Shaner, N. C., Lin, M. Z., McKeown, M. R., Steinbach, P. A., Hazelwood, K. L., Davidson, M. W., and Tsien, R. Y. (2008) Improving the photostability of bright monomeric orange and red fluorescent proteins. *Nat. Methods* **5,** 545–551
51. Kimple, A. J., Willard, F. S., Giguere, P. M., Johnston, C. A., Mocanu, V., and Siderovski, D. P. (2007) The RGS protein inhibitor CCG-4986 is a covalent modifier of the RGS4 Gα-interaction face. *Biochim. Biophys. Acta* **9,** 1213–1220
52. Stols, L., Gu, M., Dieckman, L., Raffen, R., Collart, F. R., and Donnelly, M. I. (2002) A new vector for high-throughput, ligation-independent cloning encoding a tobacco etch virus protease cleavage site. *Protein Expr. Purif.* **25,** 8–15
53. Willard, F. S., Kimple, A. J., Johnston, C. A., and Siderovski, D. P. (2005) A direct fluorescence-based assay for RGS domain GTPase accelerating activity. *Anal. Biochem.* **340,** 341–351
54. Kimple, A. J., Yasgar, A., Hughes, M., Jadhav, A., Willard, F. S., Muller, R. E., Austin, C. P., Inglese, J., Ibeanu, G. C., Siderovski, D. P., and Simeonov, A. (2008) A high throughput fluorescence polarization assay for inhibitors of the GoLoco motif/Gα interaction. *Comb Chem. High Throughput Screen* **11,** 396–409
55. Skiba, N. P., Bae, H., and Hamm, H. E. (1996) Mapping of effector binding sites of transducin α-subunit using $G\alpha_t/G\alpha_{i1}$ chimeras. *J. Biol. Chem.* **271,** 413–424
56. Yamanaka, G., Eckstein, F., and Stryer, L. (1985) Stereochemistry of the guanyl nucleotide binding site of transducin probed by phosphorothioate analogues of GTP and GDP. *Biochemistry* **24,** 8094–8101
57. Hutsell, S. Q., Kimple, R. J., Siderovski, D. P., Willard, F. S., and Kimple, A. J. (2010) High-affinity immobilization of proteins using biotin- and GST-based coupling strategies. *Methods Mol. Biol.* **627,** 75–90
58. Kimple, A. J., Muller, R. E., Siderovski, D. P., and Willard, F. S. (2010) A capture coupling method for the covalent immobilization of hexahistidine tagged proteins for surface plasmon resonance. *Methods Mol. Biol.* **627,** 91–100
59. Bosch, D. E., Zielinski, T., Lowery, R. G., and Siderovski, D. P. (2012) Evaluating modulators of "regulator of G-protein signaling" (RGS) proteins. *Curr. Protoc. Pharmacol.* **56,** 2.8.1–2.8.15
60. Johnston, C. A., Lobanova, E. S., Shavkunov, A. S., Low, J., Ramer, J. K., Blaesius, R., Fredericks, Z., Willard, F. S., Kuhlman, B., Arshavsky, V. Y., and Siderovski, D. P. (2006) Minimal determinants for binding activated Gα from the structure of a $G\alpha_{i1}$-peptide dimer. *Biochemistry* **45,** 11390–11400
61. Mall, M. A., Button, B., Johannesson, B., Zhou, Z., Livraghi, A., Caldwell, R. A., Schubert, S. C., Schultz, C., O'Neal, W. K., Pradervand, S., Hummler, E., Rossier, B. C., Grubb, B. R., and Boucher, R. C. (2010) Airway surface liquid volume regulation determines different airway phenotypes in liddle compared with βENaC-overexpressing mice. *J. Biol. Chem.* **285,** 26945–26955
62. Worthington, E. N., and Tarran, R. (2011) Methods for ASL measurements and mucus transport rates in cell cultures. *Methods Mol. Biol.* **742,** 77–92
63. Strachan, R. T., Sheffler, D. J., Willard, B., Kinter, M., Kiselar, J. G., and Roth, B. L. (2009) Ribosomal S6 kinase 2 directly phosphorylates the 5-hydroxytryptamine 2A (5-HT2A) serotonin receptor, thereby modulating 5-HT2A signaling. *J. Biol. Chem.* **284,** 5557–5573
64. Kimple, A. J., Soundararajan, M., Hutsell, S. Q., Roos, A. K., Urban, D. J., Setola, V., Temple, B. R., Roth, B. L., Knapp, S., Willard, F. S., and Siderovski, D. P. (2009) Structural determinants of G-protein α subunit selectivity by regulator of G-protein signaling 2 (RGS2). *J. Biol. Chem.* **284,** 19402–19411
65. Kosloff, M., Travis, A. M., Bosch, D. E., Siderovski, D. P., and Arshavsky, V. Y. (2011) Integrating energy calculations with functional assays to decipher the specificity of G protein-RGS protein interactions. *Nat. Struct. Mol. Biol.* **18,** 846–853
66. Soundararajan, M., Willard, F. S., Kimple, A. J., Turnbull, A. P., Ball, L. J., Schoch, G. A., Gileadi, C., Fedorov, O. Y., Dowler, E. F., Higman, V. A., Hutsell, S. Q., Sundström, M., Doyle, D. A., and Siderovski, D. P. (2008) Structural diversity in the RGS domain and its interaction with heterotrimeric G protein α-subunits. *Proc. Natl. Acad. Sci. U.S.A.* **105,** 6457–6462
67. Tesmer, J. J., Berman, D. M., Gilman, A. G., and Sprang, S. R. (1997) Structure of RGS4 bound to AlF4–activated $G_i\alpha_1$. stabilization of the transition state for GTP hydrolysis. *Cell* **89,** 251–261
68. Xu, X., Zeng, W., Popov, S., Berman, D. M., Davignon, I., Yu, K., Yowe, D., Offermanns, S., Muallem, S., and Wilkie, T. M. (1999) RGS proteins determine signaling specificity of G_q-coupled receptors. *J. Biol. Chem.* **274,** 3549–3556
69. Zheng, B., Ma, Y. C., Ostrom, R. S., Lavoie, C., Gill, G. N., Insel, P. A., Huang, X. Y., and Farquhar, M. G. (2001) RGS-PX1, a GAP for GαS and sorting nexin in vesicular trafficking. *Science* **294,** 1939–1942
70. Castellone, M. D., Teramoto, H., Williams, B. O., Druey, K. M., and Gutkind, J. S. (2005) Prostaglandin E2 promotes colon cancer cell growth through a G_s-axin-β-catenin signaling axis. *Science* **310,** 1504–1510
71. Sinnarajah, S., Dessauer, C. W., Srikumar, D., Chen, J., Yuen, J., Yilma, S.,

Dennis, J. C., Morrison, E. E., Vodyanoy, V., and Kehrl, J. H. (2001) RGS2 regulates signal transduction in olfactory neurons by attenuating activation of adenylyl cyclase III. *Nature* **409,** 1051–1055
72. Hart, M. J., Jiang, X., Kozasa, T., Roscoe, W., Singer, W. D., Gilman, A. G., Sternweis, P. C., and Bollag, G. (1998) Direct stimulation of the guanine nucleotide exchange activity of p115 RhoGEF by $G\alpha_{13}$. *Science* **280,** 2112–2114
73. Fukuhara, S., Chikumi, H., and Gutkind, J. S. (2000) Leukemia-associated Rho guanine nucleotide exchange factor (LARG) links heterotrimeric G proteins of the G_{12} family to Rho. *FEBS Lett.* **485,** 183–188
74. Heximer, S. P., Watson, N., Linder, M. E., Blumer, K. J., and Hepler, J. R. (1997) RGS2/G0S8 is a selective inhibitor of $G\alpha_q$ function. *Proc. Natl. Acad. Sci. U.S.A.* **94,** 14389–14393
75. Bansal, G., Druey, K. M., and Xie, Z. (2007) R4 RGS proteins. Regulation of G-protein signaling and beyond. *Pharmacol. Ther.* **116,** 473–495
76. Slep, K. C., Kercher, M. A., He, W., Cowan, C. W., Wensel, T. G., and Sigler, P. B. (2001) Structural determinants for regulation of phosphodiesterase by a G protein at 2.0 Å. *Nature* **409,** 1071–1077
77. Popov, S., Yu, K., Kozasa, T., and Wilkie, T. M. (1997) The regulators of G protein signaling (RGS) domains of RGS4, RGS10, and GAIP retain GTPase activating protein activity *in vitro*. *Proc. Natl. Acad. Sci. U.S.A.* **94,** 7216–7220
78. Berman, D. M., Wilkie, T. M., and Gilman, A. G. (1996) GAIP and RGS4 are GTPase-activating proteins for the G_i subfamily of G protein α subunits. *Cell* **86,** 445–452
79. Lan, K. L., Sarvazyan, N. A., Taussig, R., Mackenzie, R. G., DiBello, P. R., Dohlman, H. G., and Neubig, R. R. (1998) A point mutation in $G\alpha_o$ and $G\alpha_{i1}$ blocks interaction with regulator of G protein signaling proteins. *J. Biol. Chem.* **273,** 12794–12797
80. Cozens, A. L., Yezzi, M. J., Kunzelmann, K., Ohrui, T., Chin, L., Eng, K., Finkbeiner, W. E., Widdicombe, J. H., and Gruenert, D. C. (1994) CFTR expression and chloride secretion in polarized immortal human bronchial epithelial cells. *Am. J. Respir. Cell Mol. Biol.* **10,** 38–47
81. Rhee, S. G. (2001) Regulation of phosphoinositide-specific phospholipase C. *Annu. Rev. Biochem.* **70,** 281–312
82. Nishiyama, M., Yuki, S., Fukano, C., Sako, H., Miyamoto, T., and Tomooka, Y. (2011) Attempt to develop taste bud models in three-dimensional culture. *Zoolog. Sci.* **28,** 623–632
83. Sobolev, V., Eyal, E., Gerzon, S., Potapov, V., Babor, M., Prilusky, J., and Edelman, M. (2005) SPACE. A suite of tools for protein structure prediction and analysis based on complementarity and environment. *Nucleic Acids Res.* **33,** W39–43